The Sensitivity of an Intermediate Model of the Midlatitude Troposphere's Equilibrium to Changes in Radiative Forcing*

Amy Solomon

International Pacific Research Center, SOEST, University of Hawaii, Honolulu, Hawaii

Peter H. Stone

Department of Earth, Atmospheric and Planetary Sciences, Massachusetts Institute of Technology, Cambridge, Massachusetts

ABSTRACT

The sensitivity of the equilibrated state of a dry high-resolution quasigeostrophic β-plane channel model, coupled to both a simplified model of the atmospheric boundary layer and an interactive static stability, to changes in forcings is investigated. An earlier study with the same model found that with standard parameter values, the potential vorticity in the center of the channel just above the atmospheric boundary layer was homogenized. The new experiments show that this result is robust does not vary strongly with variations in forcing over a wide range of forcing parameters. This is so even though the meridional temperature gradients and static stability are generally sensitive to the forcing; that is, the changes in these cooperate to keep the meridional potential vorticity gradient zero. The potential vorticity gradients at higher levels are also robust although nonzero. The homogenization in the lower troposphere does disappear if the differential diabatic heating is decreased sufficiently or if the tropopause level is lowered sufficiently.

The model results are also used to assess proposed parameterizations of eddy effects. Stone's parameterization of the meridional eddy heat flux is most successful at reproducing the model's results for most of the experiments. However, no parameterizations of the eddy heat flux captured the results of the experiments in which the diabatic heating timescale was varied. In these experiments, changes in the eddy heat fluxes kept the tropospheric temperature structure essentially unchanged even though the timescale changed from 5 to 80 days.

1. Introduction

Cehelsky and Tung (1991) and Welch and Tung (1998) used a two-layer quasigeostrophic β-plane model to study the dynamical processes by which the midlatitude atmosphere equilibrates. They found that if the forcing is strong enough, the initially most unstable wave will saturate causing longer less unstable waves to dominate the heat transport in the equilibrated state. They also found that the equilibrated state of their model was linearly stable to the dominant heat transporting mode, which was a function of the forcing. Therefore, the equilibrated state of their model was sensitive to the forcing even though the dynamics were quasi-linear, because the equilibrated state determined by the longer waves had meridional temperature gradients that were

Corresponding author address: Dr. Amy Solomon, International Pacific Research Center, SOEST, University of Hawaii, 1000 Pope Road, Honolulu, HI 96822.
E-mail: amy@iprc.soest.hawaii.edu

larger than the equilibrated state that would have resulted if the most unstable wave had not saturated. The term quasi linear is used to describe dynamics that are governed by wave–mean flow interactions.

Recently, we developed a model similar to Welch and Tung's except that it has much higher vertical resolution, an interactive static stability, and a simple model of the atmospheric boundary layer (ABL) (Solomon and Stone 2001, hereafter SS). These refinements make it possible for the model to simulate the different dynamical balances present in the vertical structure of the troposphere, as discussed by Stone and Nemet (1996). In particular, the troposphere appears to be divided into an ABL dominated by dissipative processes, a lower troposphere where baroclinic eddy processes dominate and tend to homogenize the potential vorticity (PV), and an upper troposphere that is closer to radiative–convective equilibrium. These different regimes are not resolved in two-layer models. Solomon and Stone studied how this vertical structure is maintained and found results similar to Cehelsky and Tung's and Welch and Tung's (e.g., the dynamics is essentially quasi-linear), but SS did not vary the forcing.

The ideas and model results discussed above motivate

the questions we explore in this study. Do the two-layer model results for how equilibration depends on the forcing still apply when higher vertical resolution is used? Are SS's results for how the vertical structure is divided into different regimes independent of the forcing? These are important questions because if it can be shown that the equilibrated state or some of its aspects are relatively insensitive to changes in forcings, then they can be prescribed without simulating the dynamics explicitly. We explore these questions by investigating how the equilibrated state discussed in SS varies as the forcing is varied. From these model runs, it will be possible to determine what aspects of the equilibrated state are robust. The dynamical processes are also explored more fully by a series of runs that test how perturbing the equilibrated state modifies the stability characteristics of the mean state.

The structure of this paper is as follows. Section 2 briefly describes the model used in this paper. Section 3 presents and discusses the results of the nonlinear model runs, which test the sensitivity of the equilibrated state of SS to changes in the radiative forcing. Section 4 presents the spectral and stability characteristics of the equilibrated states and how they vary with the forcing. Section 5 compares our numerical model results with various parameterizations that have been proposed for simulating eddy effects. Section 6 summarizes the results and discusses the implications of this study for understanding the processes that maintain the temperature structure of the midlatitude troposphere.

2. The model

a. Fully nonlinear quasigeostrophic model

The model used in this study is described in detail in SS. The quasigeostrophic equations on a β plane centered at 45° latitude are coupled to an equation for the vertical structure of the horizontally averaged potential temperature and a simple model of the ABL. All model runs have a channel width of 10 000 km and a channel length of 21 040 km. The horizontal grid length is approximately 300 km in both the zonal and meridional directions (65 and 33 grid points, respectively). There are 17 equally spaced pressure levels, with a grid spacing of 62.5 hPa.

Diabatic heating is parameterized in this model by a relaxation back to a radiative convective equilibrium state with a constant diabatic heating timescale. The diabatic heating timescale, τ_d, in the standard model is set equal to 40 days. The radiative convective equilibrium (RCE) state is represented by a horizontally averaged mean lapse rate, $-dT_r/dz$, plus horizontal temperature gradients, dT_r/dy. The lapse rate in radiative convective equilibrium in the standard run (SR) is chosen to be a constant 7.0 K km^{-1} in the troposphere. The lapse rate at all levels in the stratosphere (250 hPa and higher in SR) is taken to be 0. The radiative equilibrium

TABLE 1. Experiments carried out to determine the sensitivity of the equilibrated climate to changes in forcing. Blank spaces denote parameters equal to the standard run. Runs that were done to determine the sensitivity of the equilibrated climate to changes in forcing. Blank spaces denote parameters equal to the standard run.

Run	$d\theta_r/dy$ K (1000 km)$^{-1}$	dT_r/dy K (1000 km)$^{-1}$	dT_r/dz K km^{-1}	Jet 1000 km	S–T Standard	τ_d Days
SR	−13.2	*****	−7.0	5.0	Yes	40
TY1	−23.2					
TY2	−17.8					
TY3	−16.1					
TY4	−14.7					
TY5	−12.1					
TY6	−11.0					
TY7	−6.7					
TY8	*****	−13.2				
TZ1			−9.0			
TZ2			−8.0			
TZ3			−6.0			
TZ4			−5.5			
NJT				3.3		
WJT				6.7		
SR	−13.2	*****	−7.0	5.0	Yes	40
RST					No	
LST					No	
TAU1						5
TAU2						10
TAU3						20
TAU4						60
TAU5						80

lapse rate would be much larger, closer to 15 K km^{-1} in the troposphere. Since all moist processes have been neglected in this model, the modification of the radiative equilibrium profile by moist convection is taken into account implicitly by assuming that moist convection decreases the RCE lapse rate.

The horizontal temperature gradients in radiative convective equilibrium in SR are estimated from Manabe and Möller (1961). The latitudinal temperature distribution is chosen such that the potential temperature gradients are constant with height,

$$\theta(y, p) = -21.5 \sin(\pi(y - 0.5L)/(0.5L)),$$

for $0.25L \leq y \leq 0.75L$, where L is the total channel width, 10 000 km; p is pressure; and θ is potential temperature. This gives a temperature contrast of 30 K over the center 2500 km of the channel compared to an estimate of 34 K for the wintertime temperature gradients in the lower troposphere from Manabe and Möller (1961). A region with 0 temperature gradients is extended 2500 km to the north of $y = 0.75L$ and south of $y = 0.25L$ to insure that the channel walls do not modify the dynamics. In the stratosphere in the SR, the meridional temperature gradient at all levels (250 hPa and higher in SR) is taken to be a tenth of the magnitude of the gradient 2 levels below the stratosphere (375 hPa in SR) and of opposite sign, that is, the gradient in the stratosphere is positive. The gradient at the intermediate

TABLE 2. Characteristics of the equilibrated states at the center of the channel of the fully nonlinear runs with different forcings.

Run	dT_e/dy K (1000 km)$^{-1}$	$d\theta_e/dz$ K km^{-1}	EKE m^2 s^{-2}	ENS 10^{-10} s^{-2}	$[\overline{v^*\theta^*}]^{pt}$ m K s^{-1}	$[\overline{v\theta}]^{pt}$ m K s^{-1}	$[\overline{W^*T^*}]^t$ 10^{-2} K Pa s^{-1}
SR	−6.2	4.0	317.7	25.9 (250)	18.5	−2.6	−33.6
TY1(−23.2)	−11.2	7.7	955	53.4 (250)	52.6	−3.8	−94.2
TY2(−17.8)	−9.2	5.7	575	37.4 (250)	35.2	−3.5	−64.4
TY3(−16.1)	−7.8	4.5	440	31.2 (250)	21.2	−3.8	−45.4
TY4(−14.7)	−6.5	4.7	400	30.8 (250)	18.7	−3.4	−38.9
TY5(−12.1)	−6.0	3.4	330	28.6 (250)	14.1	−2.5	−22.8
TY6(−11.0)	−5.0	2.8	104	11.2 (250)	8.6	−1.9	−19.4
TY7(−6.7)	−4.0	2.1	35	3.6 (250)	3.7	−1.2	−7.9
TY8(−13.2)	−6.1	4.1	400	30.7 (250)	22.2	−3.5	−37.2
TZ1(−9.0)	−7.9	2.8	329	36.6 (250)	17.8	−0.9	−51.7
TZ2(−8.0)	−7.2	3.4	317	29.2 (250)	18.2	−1.9	−41.4
TZ3(−6.0)	−6.0	4.4	258	21.8 (250)	18.3	−3.9	−32.3
TZ4(−5.5)	−6.0	4.7	201	17.3 (250)	16.9	−3.9	−30.1
WJT(6.7)	−7.0	4.6	430	30.8 (250)	24.3	−3.1	−38.7
NJT(3.3)	−5.2	3.2	151	17.6 (250)	11.6	−2.2	−29.4
SR	−6.2	4.0	317.7	25.9 (250)	18.5	−2.6	−33.6
RST	−5.3	4.1	412	29.2 (188)	22.1	−2.7	−32.5
LST	−7.0	3.8	207	22.6 (313)	15.5	−2.9	−36.7
TAU1(5)	−6.3	3.9	568	39.2 (250)	38.5	−3.2	−47.2
TAU2(10)	−6.3	4.0	487	35.4 (250)	31.7	−3.0	−42.7
TAU3(20)	−6.1	4.0	411	31.6 (250)	24.7	−2.8	−37.4
TAU4(60)	−6.6	3.9	241	21.6 (250)	15.5	−2.5	−33.8
TAU5(80)	−6.5	3.8	195	19.3 (250)	14.3	−2.6	−33.8

level (312.5 hPa in SR) is interpolated from the values immediately above and below.

The lower boundary is assumed to be a sea surface with fixed temperature, θ_{sea}. A linearized bulk aerodynamic drag formula is used to calculate the surface heat flux,

$$F_{\text{SH}} = -c_d c_p \rho_s |\mathbf{v}_s|(\theta_{\text{air}} - \theta_{\text{sea}}),$$

where ρ_s is the surface density. The surface air temperature θ_{air} is assumed to be equal to the potential temperature at the first level, which is 31 hPa over the surface. The drag coefficient, $c_d|\mathbf{v}_s|$, is chosen to be equal to 3×10^{-2} m s^{-1}. This is closer to estimates of drag over land than over ocean but was chosen because the resultant mean state and fluxes closely approximated observations. The sensitivity of the results to the dissipative parameters such as this will be investigated in a subsequent paper.

Above the surface, the turbulent heat fluxes in the boundary layer are assumed to be diffusive in nature and are parameterized as

$$F_{\text{SH}} = \nu_T(p)\rho^2 g c_p \frac{\partial\theta}{\partial p}, \qquad \nu_T(p) = 5\left(\frac{p}{p_0}\right)^3 \text{ m}^2 \text{ s}^{-1},$$

where p_0 is the pressure at the lower boundary. The heating effect of the vertical diffusion by the turbulent eddies is then calculated from the fluxes as

$$\frac{\partial\theta}{\partial t} = \frac{g}{c_p}\frac{\partial F_{\text{SH}}}{\partial p}.$$

A dry convective adjustment is applied to the horizontally averaged potential temperature if the temperature profile is calculated to be statically unstable. This adjustment is only necessary within the boundary layer where the mixing by the turbulent fluxes can cause the flow to become statically unstable.

Friction is parameterized by a linearized bulk aerodynamic drag at the surface and diffusive mixing above the surface in the same way as was outlined for the turbulent heating. The linearized bulk aerodynamic drag formula is used to calculate the wind stress at the surface,

$$\boldsymbol{\tau}_s = -c_d \rho_s |\mathbf{v}_s|(\mathbf{v}_g + \mathbf{v}_a),$$

where $\mathbf{v}_g$ is the geostrophic component of the wind and $\mathbf{v}_a$ is the ageostrophic component, calculated following Bannon and Salem (1995). The surface drag times the ambient surface wind, $c_d|\mathbf{v}_s|$, is again set equal to 3×10^{-2} m s^{-1}.

Above the surface, the turbulent shear stress is calculated using a flux-gradient formulation,

$$\boldsymbol{\tau}_M = \rho(\overline{\mathbf{v}^*\omega^*}) = \nu_M(p)\rho^2 g \frac{\partial(\mathbf{v}_g + \mathbf{v}_a)}{\partial p},$$

where

$$\nu_M(p) = 5\left(\frac{p}{p_0}\right)^3 \text{ m}^2 \text{ s}^{-1}.$$

Stars are used to designate deviations from the zonal mean. The vertical diffusion of momentum by the turbulent eddies is then calculated from the shear stress as $\mathbf{F} = g(\partial\boldsymbol{\tau}_M/\partial P)$.

b. Linear stability analysis

The maintenance of the equilibrated mean state will be explored with the help of a linear stability analysis (LSA). The fully nonlinear model discussed in the previous section is linearized about the time-averaged zonally averaged state and then integrated forward in time, following Jin and Hoskins (1995). All of the forcings used in the fully nonlinear model are linear and are therefore included in the LSA. The static stability is held fixed at the values taken from the nonlinear model run. The growth rate and real phase speeds of these perturbations are calculated following Gall (1976). The growth rate is calculated from the kinetic energy

$$kc_i = \frac{1}{2K_e}\frac{dK_e}{dt},$$

where K_e is the total eddy kinetic energy of the wave. The real part of the phase speed is calculated as

$$c_r = [k(\psi_s^2 + \psi_c^2)]^{-1}\left(\psi_c\frac{\partial\psi_s}{\partial t} - \psi_s\frac{\partial\psi_c}{\partial t}\right),$$

where ψ_s and ψ_c are the Fourier coefficients of the perturbation streamfunction, ψ.

3. Forcing experiments

Forcing in this model is parameterized with a linear Newtonian relaxation back to a radiative–convective equilibrium temperature structure with a diabatic heating timescale, which is independent of height. Since we specify not only the horizontal but also the vertical temperature structure of the forcing, there are many parameters and profiles that must be explored in order to get a complete picture of the forcing parameter space. The goal of this section is to get an idea of the sensitivity of the model's climate without exploring the whole parameter space. Therefore, only a few runs for each parameter and profile will be discussed. Table 1 lists the runs that we have carried out.

The terms $d\theta_r/dy$ and dT_r/dy specify the meridional temperature gradients in the RCE state at the center of the channel at the first model level (937.5 hPa). If there are numbers in the $d\theta_r/dy$ column, then the potential temperature gradients are constant with height in the troposphere. If there are numbers in the dT_r/dy column, then the temperature gradient is constant with height in the troposphere. These two different ways of specifying the temperature gradients have been used to look at how the eddy dynamics depend on the vertical structure of the temperature gradients. The term dT_r/dz is the vertical temperature gradient in the troposphere in RCE and is constant with height. "Jet" refers to the width of the jet in RCE. The number in this column is the width of the jet in units of 10^3 km. The term τ_d is the diabatic heating timescale in units of days. The term S–T refers to whether or not the run has the standard representation

of a stratosphere and a tropopause. We will not change the algorithms for prescribing the RCE structure in the stratosphere from those used in the standard run but will change the height of the RCE tropopause, that is, the height at which the algorithms are applied.

The different runs are separated into six sections. The first section looks at the sensitivity of the model's equilibrated state and fluxes to changes in the RCE meridional temperature gradients. The first seven runs TY1–TY7 vary the meridional gradients from roughly two times those in the standard run to half those in SR. TY8 looks at the sensitivity to changes in the vertical structure of the RCE meridional temperature gradients. This run has the same RCE meridional temperature gradients as SR at the surface but has temperature gradients that are independent of pressure rather than potential temperature gradients as in SR. The second section varies the RCE lapse rate from -5.5 K km^{-1} to -9 K km^{-1}, runs TZ1–TZ4. The third section looks at the sensitivity to the meridional extent of the RCE jet structure, runs NJT and WJT. NJT and WJT vary the meridional extent of the jet while keeping the meridional temperature gradients at the center of the channel equal to those in the control run. WJT has a jet that is 1.33 times the width of the jet in the control run. NJT has a jet that is 0.67 times the width of the jet in the control run. The fourth section looks at the sensitivity to changes in the height of the tropopause, runs RST and LST. RST has an RCE stratosphere with its first level at 187.5 hPa, while the RCE stratosphere in LST has its first level at 312.5 hPa. The last section looks at the sensitivity to changes in the diabatic heating timescale, runs TAU1–TAU5. All the experiments are integrated for 1000 days, and statistics are calculated for the last 800 days.

Table 2 lists some characteristics of the equilibrated state at the center of the channel for each run. The term dT_e/dy is the minimum equilibrated temperature gradient at the three levels between 750–850 hPa. The term $d\theta_e/dz$ is the maximum static stability between 750–850 hPa. EKE is the value of the eddy kinetic energy at the level where it peaks. ENS is the value of the eddy enstrophy at the level where it peaks. Also shown in parentheses are the pressure levels at which the EKE and ENS peaks are located, in units of hectopascals. The terms $[v^*\theta^*]^{p,t}$ and $[\overline{v}\overline{\theta}]^{p,t}$ are the time-averaged vertically averaged eddy meridional potential temperature fluxes and mean meridional potential temperature fluxes, respectively. The term $[\overline{W^*T^*}]^t$ is the minimum (i.e., maximum magnitude) of the vertical eddy temperature flux. Stars are used to designate deviations from the zonal mean, bars designate zonal averages, and brackets designate averages over the variables listed in the upper right.

a. Equilibrated state

Figure 1 shows a comparison of the PV gradients for the runs listed in Table 1. If we assume $\partial^2\overline{u}/\partial y^2$ is small,
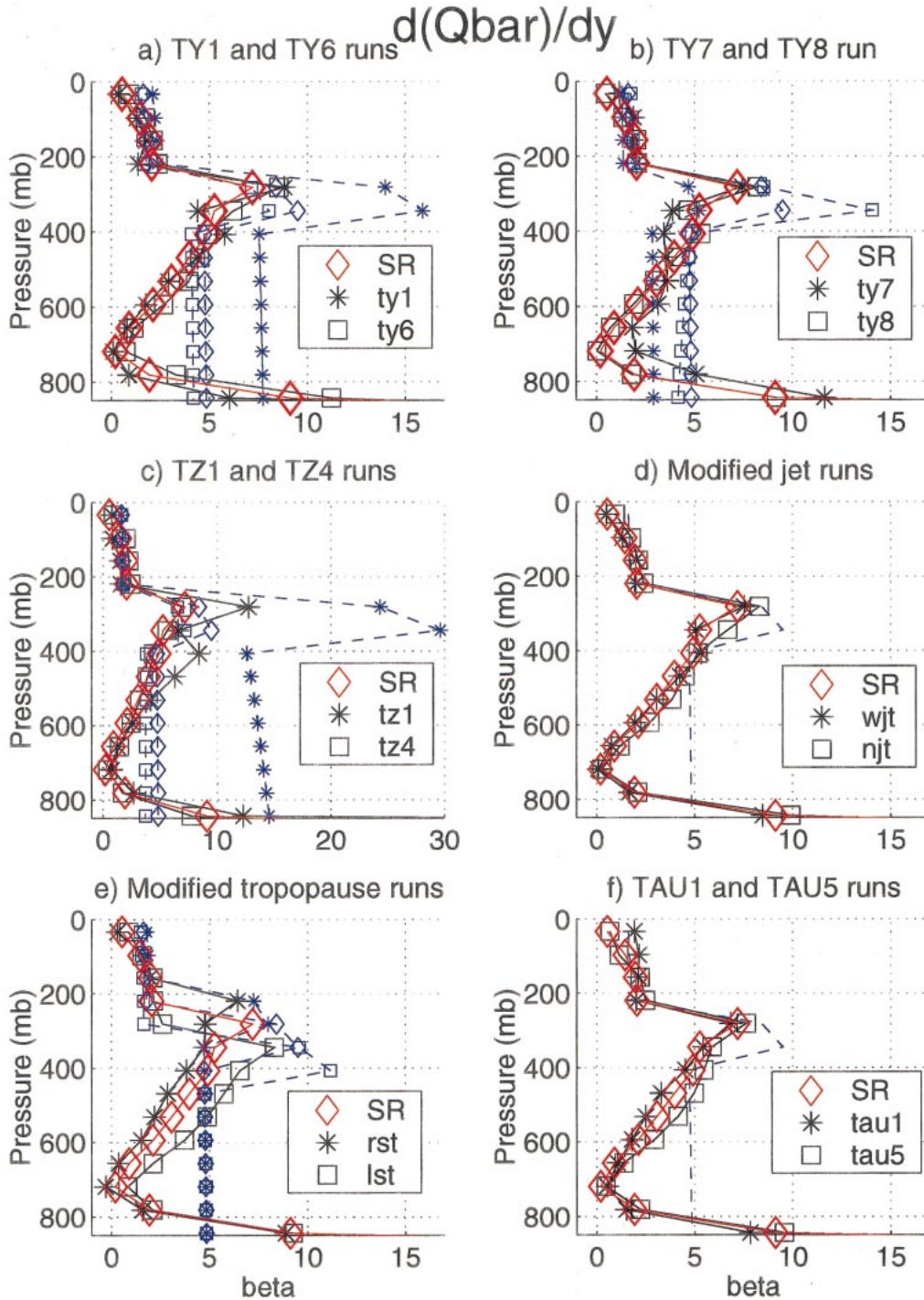
FIG. 1. Comparison of the equilibrated PV gradients at the center of the channel for runs that modify radiative forcing, in units of β. Dashed lines indicate the RCE profiles.

these are proportional to the vertical derivative of the slope of the isentropes, S_p, plus β. The results are plotted as solid lines separately for each section in Table 1. The dashed lines show what the gradients would be in RCE. The solid lines show that the equilibrated PV gradients are relatively robust, considering the large variations in

the forcings, that is, in the RCE gradients. This is also true in two-layer models (Stone and Branscome 1992; Zhou and Stone 1993a,b).

In all of our runs, it is S_p that is found to be a robust field, not S itself. This distinction cannot be made in two-layer models because of their low vertical resolu-
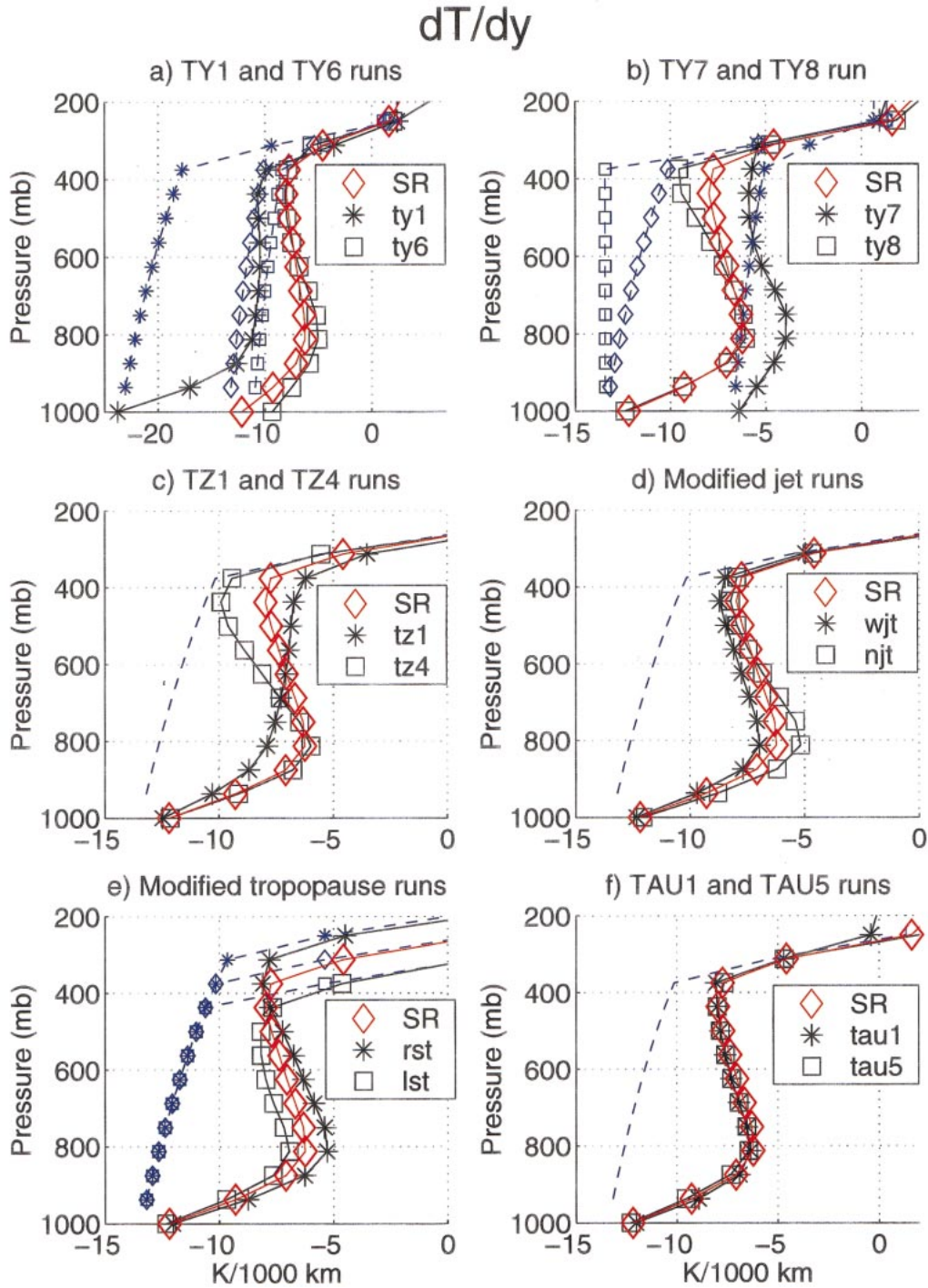
FIG. 2. Comparison of the equilibrated meridional temperature gradients at the center of the channel for runs that modify radiative forcing [in units of K $(1000 \text{ km})^{-1}$]. Dashed lines indicate the RCE profiles.

tion. If PV is completely homogenized and $\partial^2 u/\partial y^2$ is negligible, then in this model, S_p would be a constant. This is clearly not the case because PV is only homogenized above the ABL between 600–750 hPa. Indeed, at the 719 hPa level, the PV gradient is essentially 0 in all the runs except TY7 and LST. The PV gradients at

other levels are also very robust (except for the TZ1, TY7, RST, and LST runs) but are nonzero. The structure is similar to that in the atmosphere (Stone and Nemet 1996).

Figures 2 and 3 compare plots of dT_e/dy and $d\theta_e/dz$ for the same runs as Fig. 1. These figures show that the
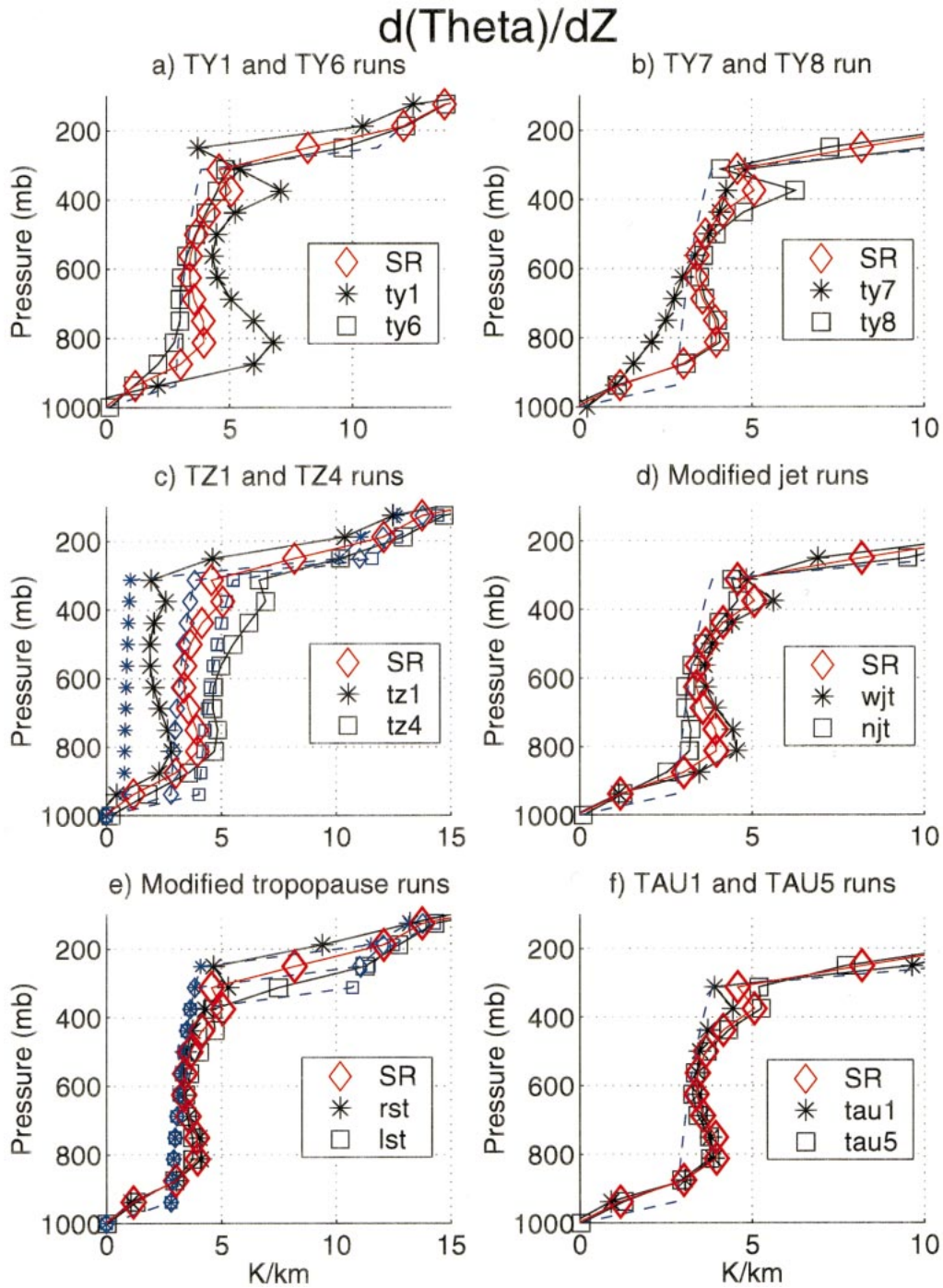
FIG. 3. Comparison of the equilibrated static stability at the center of the channel for runs that modify radiative forcing (in units of K km^{-1}). Dashed lines indicate the RCE profiles.

equilibrated profiles of $d\theta_e/dz$ and dT_e/dy are not as robust as the PV gradients. There is no clear division of adjustment between dT_e/dy and $d\theta_e/dz$. This is because S_p is the vertical derivative of the slope of the isentropes, so the robust profile seen in Fig. 1 can be accomplished by a wide variety of $d\theta_e/dz$ and dT_e/dy

profiles. The term dT_e/dy is more sensitive to the forcing than in two-layer models with fixed static stability, but the sensitivity is similar to that in two-layer models with variable static stability (Zhou and Stone 1993a,b).

Table 2 shows the vertically integrated meridional and vertical eddy heat fluxes for all the runs. These numbers
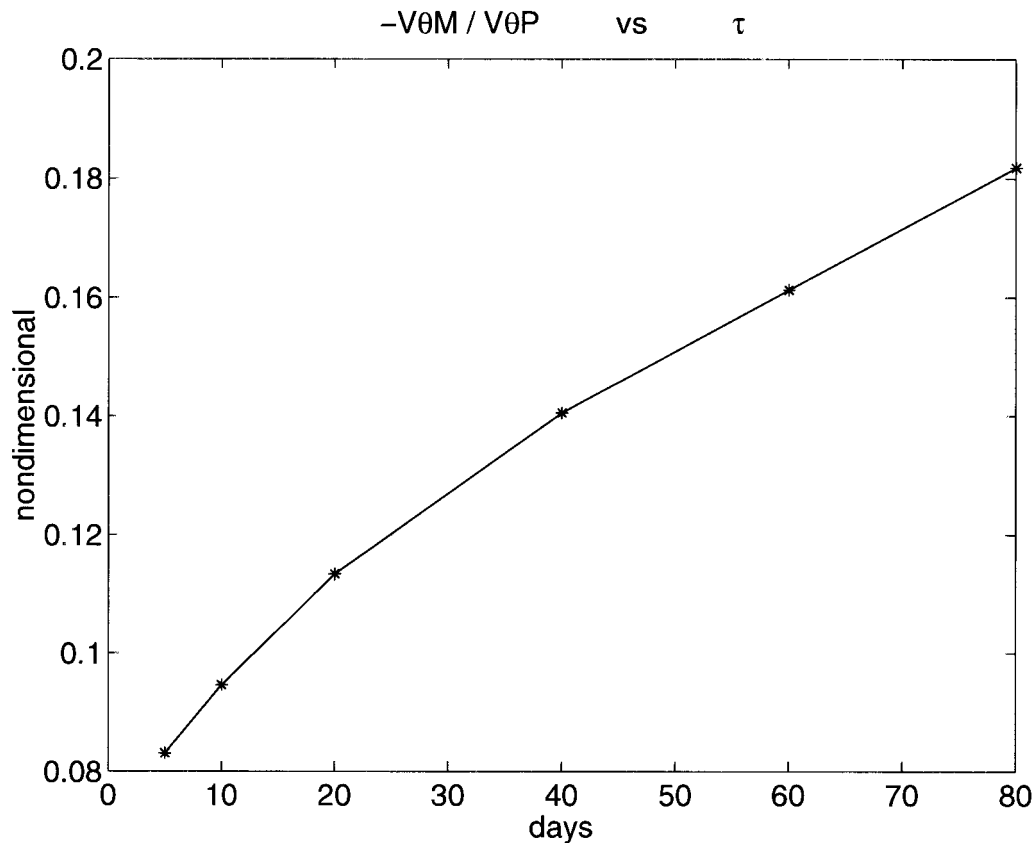
FIG. 4. Ratio of mean and eddy meridional potential temperature fluxes vs the diabatic heating timescale τ. These results are from runs TAU1–TAU5 and SR.

show that an increase in the temperature gradients across the channel results in increased meridional as well as vertical eddy heat fluxes, whereas changes in the static stability only cause small changes in the meridional eddy heat flux while causing substantial changes in the vertical eddy heat flux. These results show that the same adjustment to the PV gradients is accomplished in two very different ways when the RCE lapse rate is decreased and when the RCE meridional temperature contrast is increased. For example, comparing TY2 to TZ1, it is seen that the two runs have essentially the same equilibrated PV gradient distribution but very different equilibrated lapse rates and meridional temperature gradients. The different ways of attaining the equilibrated S_p can also be seen in a comparison of the EKE for the runs (Table 2). Varying the lapse rate results in small changes in the EKE relative to the large changes that result when the meridional temperature contrast is varied.

b. Varying the jet width

The SR has a RCE jet that is 5000 km wide. This distance is very close to the wavelength of typical unstable waves. Previous wave–mean flow studies have shown that a potentially important equilibration process

is the barotropic governor (James 1987). The waves equilibrate not only by reducing the shear but also by modifying the barotropic structure of the mean jet. Changing the jet structure may result in a large change in the eddy fluxes. In order to determine whether the results of the SR are robust and relatively independent of the imposed jet width, the model has been run with an RCE jet width of 6700 km, run WJT, and an RCE jet width of 3300 km, run NJT. The temperature gradients at the center of the channel are chosen to be equal to those of the SR. The wider jet has a temperature difference of 53.7 K across the center 5000 km of the channel compared to 43 K in the SR.

Table 2 shows that the meridional eddy heat fluxes in the equilibrated state of WJT are twice as large as those in NJT. Figures 2d and 3d show that equivalent changes in the static stability and the meridional temperature gradients at the center of the channel result in PV gradients at the center of the channel that are insensitive to the change in the structure of the RCE jet structure (Fig. 1d). Therefore, a tightening of the RCE jet stabilizes the waves and results in smaller fluxes and less of an adjustment to the static stability and more of an adjustment to the meridional temperature gradients, even though the equilibrated PV gradients at the center of the channel remain the same.
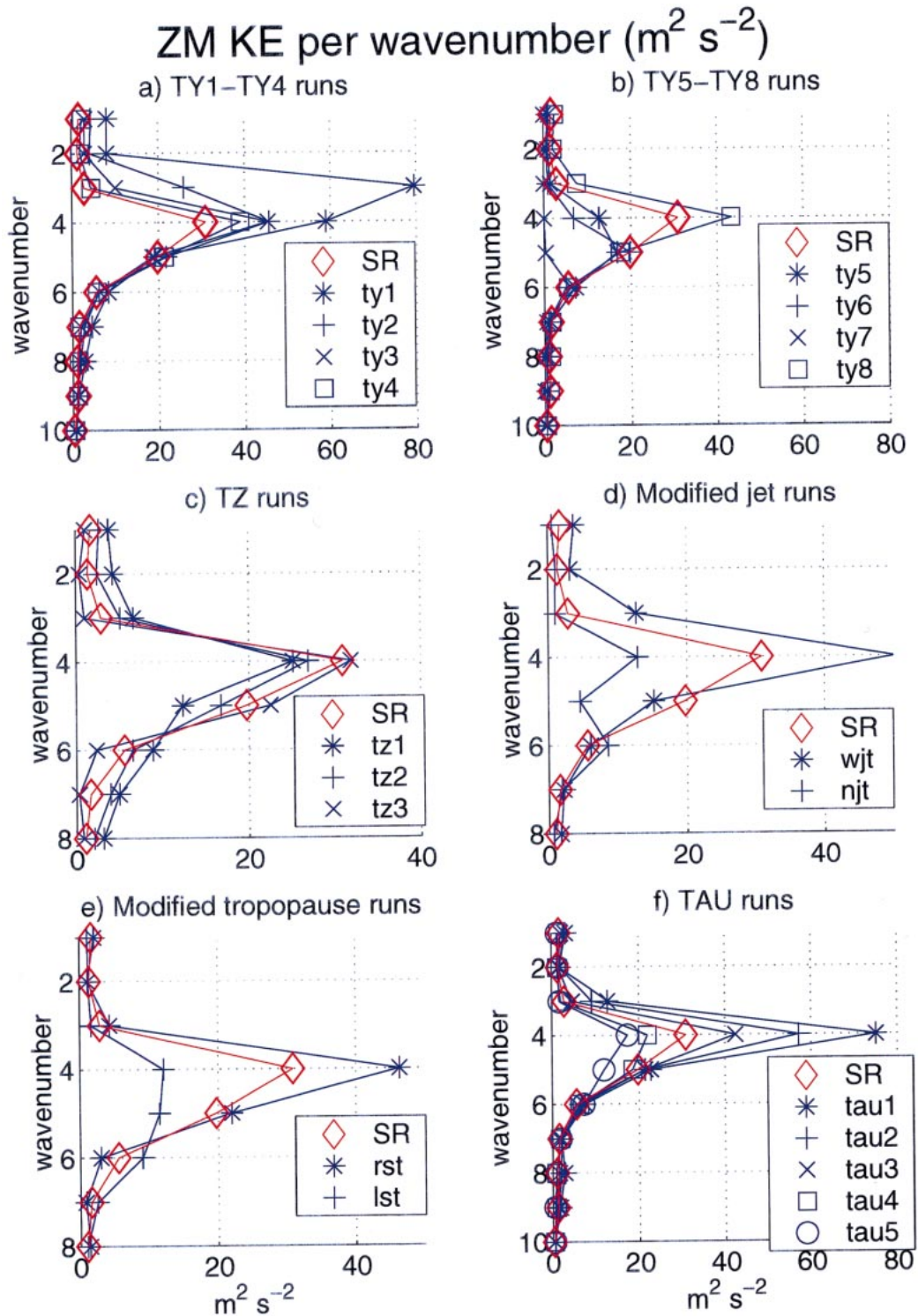
ZM KE per wavenumber (m^2 s^{-2})

FIG. 5. Comparison of the equilibrated mean volume-averaged kinetic energy per wavenumber (in units of m^2 s^{-2}).

c. Varying the vertical structure of dT/dy

TY8 has been run to test the sensitivity of the equilibrated state to changes in the vertical structure of the RCE temperature structure. The potential temperature gradients of the SR are constant with height. TY8 holds the temperature gadients constant with height. The temperature contrast at the surface is equal to 43 K over the center 5000 km of the channel for both TY8 and SR. Therefore, the temperature gradient of the SR decreases with height, and the contrast over 5000 km is equal to -30.8 K at 312 hPa. This is a 28% reduction in the magnitude of the temperature gradients in the upper troposphere. This vertical structure has been chosen as a simple comparison with the SR and as a test of the sensitivity of the temperature structure in the lower troposphere to changes in the RCE temperature structure in the upper troposphere.

Table 2 shows that the increased meridional temperature gradients result in increased EKE and eddy fluxes by approximately 20%. Figure 2b shows that the equilibrated state of TY8 has a larger magnitude of the meridional temperature gradients than the SR in the upper troposphere. Figure 3b shows that there is an increase in the static stability in the upper troposphere, making the PV gradients insensitive to the change in the vertical structure of the forcing (Fig. 1b).

d. Varying the height of the RCE tropopause

Figure 1e shows that varying the height of the RCE tropopause, that is, the height at which the lapse rate becomes 0, has the largest impact on the PV gradients above the ABL. This is very interesting considering that the forcing is only being varied above 344 hPa. It is also interesting to note how small the adjustments to the temperature structure have to be (Figs. 2e and 3e) to have large changes in the PV gradients (large here meaning on the order of β) and just how small the changes to the PV gradients are for the other series of runs that have been done. It appears that the PV gradients increase quasi linearly from the homogenized region just above the ABL to the tropopause, the location of which is determined by the forcing in this model. This is true for all of the runs done in this study.

Table 2 shows that raising the height of the RCE tropopause increases the EKE at the tropopause and the vertically integrated $[\overline{v^* \theta^*}]^{pt}$. It is actually lowering the RCE tropopause that reduces the EKE at the tropopause and the vertically integrated $[\overline{v^* \theta^*}]^{pt}$. Table 2 also shows that varying the height of the tropopause results in changes in the lower troposphere meridional temperature gradients, while the static stability in the lower troposphere is relatively unchanged. This is very different from the previous runs discussed, which had adjustments to both the meridional temperature gradients and the static stability, which inhibited changes in the PV gradients in response to the change in forcing. This

suggests that changing the height of the RCE tropopause results in a modified equilibrated PV structure in contrast to variations in the RCE meridional temperature gradients, RCE static stability, and diabatic heating timescale (next section).

e. Varying the diabatic heating timescale

Figures 1f, 2f, and 3f show that the equilibrated PV and temperature distribution are relatively insensitive to a change in the diabatic heating timescale, τ. Figure 4 plots the ratio of the magnitudes of the mean and eddy meridional heat fluxes, R, versus τ. In diabatically forced quasigeostrophic eddy regimes, R is a measure of how strongly eddies force the mean flow: if $\tau \to 0$, then $R \to 0$, and the eddy forcing is very strong; if $\tau \to \infty$, then $R \to 1$, and there is no forcing, that is, the divergence of the Eliassen–Palm flux is 0 (Stone and Branscome 1992). Figure 4 shows how R varies as τ varies in our study. It remains small, that is, the eddy forcing is strong throughout the range of τ we have studied. The values of R are somewhat smaller than those in two-layer models, but the sensitivity to τ is similar to that found when an interactive static stability is included in the two-layer model (Zhou and Stone 1993b).

4. Spectral and stability characteristics

Figure 5 shows the zonal wavenumber spectrum of the equilibrated mean kinetic energy from all our experiments. Figures 5a,b show how the spectrum varies as the conventional measure of forcing, TY, is changed. We see that even for the weakest forcing case, TY7, wavenumber 6 is already saturated, that is, increasing the forcing does not lead to any further increase in the wave's amplitude. Wavenumber 5 saturates in TY5, but wavenumber 4 has still not saturated even for our strongest forcing case, TY1. The zonal wavenumber where the kinetic energy peaks shifts from 6 in TY7 to 3 in TY1 is consistent qualitatively with Welch and Tung's (1998) two-layer model results.

Figure 5c shows that changing the static stability of the RCE has relatively little impact on the kinetic spectrum. Narrowing the RCE jet and lowering the RCE tropopause decreases the kinetic energy per wavenumber (Figs. 5d,e). Increasing the diabatic heating timescale results in a monotonic decrease in the kinetic energy per wavenumber, leaving the wavenumber at which the kinetic energy peaks unchanged (Fig. 5f).

Table 3 shows the results of our analysis of the stability of the zonal mean basic state averaged over 800 days for all of the runs. This table shows that many of the runs are linearly unstable about the averaged zonal mean basic state, although the instability is generally very weak (except for run TZ1). Looking at the runs that vary the meridional temperature gradients (TY1–TY7), we see that the stability characteristics vary smoothly with the changes in forcing. Runs TY1 and

TABLE 3. Growth rates and phase speeds of the linearly unstable waves from the LSAs (in units of day^{-1} and m s^{-1}, respectively).

Run	Unstable waves	c_i day^{-1}	c_r m s^{-1}
SR	None		
TY1(−23.2)	5	0.023	13.9
TY2(−17.8)	5	0.031	10.9
TY3(−16.1)	None		
TY4(−14.7)	None		
TY5(−12.1)	6	0.007	8.7
TY6(−11.0)	6	0.023	7.6
TY7(−6.7)	None		
TY8(−13.2)	None		
TZ1(−9.0)	6	0.142	10.7
	7	0.147	10.9
TZ2(−8.0)	6	0.063	9.6
TZ3(−6.0)	None		
TZ4(−5.5)	None		
WJT(6.7)	None		
NJT(3.3)	6	0.018	7.6
SR	None		
RST	None		
LST	6	0.026	8.8
TAU1(5)	None		
TAU2(10)	None		
TAU3(20)	None		
TAU4(60)	6	0.005	9.0
TAU5(80)	6	0.025	8.6

TY2, the runs with the strongest forcing, are linearly unstable to wave 5. Reducing the forcing stabilizes wave 5 (TY3 and TY4). Reducing the forcing further results in an unstable wave 6, runs TY5 and TY6. Reducing the forcing further causes wave 6 to become linearly stable. Runs TY1, TY2, TY5, and TY6 have linearly most unstable waves, which have become saturated (see Fig. 5a). This is also the case when the diabatic heating timescale is decreased.

In order to explore these results further, a series of quasi-linear integrations were run for SR, TY1, TY7, TAU1, and TZ1. The quasi-linear runs have static stability fixed at the equilibrated nonlinear values and have all wave–wave advective terms removed from the tendency equations. The integrations are started in radiative–convective equilibrium. Figures 6 and 7 show the results from this series of runs. Figure 6 is a comparison of the time-averaged volume-averaged perturbation potential vorticity amplitude per wavenumber, $[\overline{q^{*2}(k)}]^{y,p,t}$, for the quasi-linear and nonlinear runs, while Fig. 7 shows a comparison of the time-averaged volume-averaged total and wave–mean flow PV fluxes per wavenumber, $[\overline{v(k)q(k)}]^{y,p,t}$ and $[\overline{v^*(k)q^*(k)}]^{y,p,t}$, from the nonlinear runs.

Figure 6a shows that for the standard run (SR) the wave with the largest kinetic energy in the fully nonlinear run (wave 4) is stable in the quasi-linear integration. The quasi-linear integration is essentially maintained by wave 5 alone. Looking at Fig. 7a, we see that wave 4 grows primarily due to wave–mean flow interaction and that the wave–wave interactions on balance

reduce the amplitude of the most active waves. However, as we showed in our earlier study (SS), in the fully nonlinear case, the upscale energy cascade is essential to maintaining wave 4 in SR.

Figures 6b and 7b show that the increased forcing in TY1 destabilizes wave 4 and causes wave 5 to saturate, consistent with the results presented in Table 8. Similar to wave 4 in SR, wave 3 in TY1 grows primarily due to wave–mean flow interaction even though it is stable in the quasi-linear integration. The results from this study are different from Welch and Tung (1998) in that the smaller-scale waves are always linearly stable. Figures 6c and 7c show that the decreased forcing in TY7 essentially eliminates the wave–wave interactions and the upscale energy cascade. Figures 6d and 7d show that decreasing the diabatic timescale increases the upscale energy cascade and the amplitude of the unsaturated waves even though the time-averaged equilibrated basic state is stable for all waves (Table 3). Figures 6e and 7e show that decreasing the static stability (TZ1) destabilizes shorter waves, which saturate (Fig. 5c).

Figures 5, 6, and 7 demonstrate that changing the radiative forcing does affect which waves are linearly unstable and which waves saturate. The question remains, what causes the equilibrated PV gradients at the center of the channel to be insensitive to the changes in forcing? The answer appears to be that the nonlinear dynamics shift the spectrum and wave–mean flow interactions to larger scales, and the longer waves interact sufficiently strongly with the mean flow to stabilize all waves by wiping out the PV gradient at the steering level or nearly so. This occurs in all our nonlinear runs except TY7 and LST, and in all these runs, the perturbation PV peaks at zonal wavenumber 4, independent of the scale of the wave that dominates the quasi-linear integrations. All these runs (again except TY7 and LST) eliminate the PV gradients at the center of the channel just above the ABL (see Fig. 5). By contrast, the forcing in TY7 is too weak for these nonlinear shifts to come into play (see Figs. 6c and 7c), and in LST, they are sufficiently weak that the nonlinear effects are not as strong as in the other runs (see Figs. 6f and 7f); correspondingly, the potential vorticity is not homogenized in these two runs (see Fig. 5).

5. Parameterizations of eddy effects

Our experiments afford us an opportunity to test various methods proposed for parameterizing the effects of eddies. One class of parameterizations relates the eddy heat flux to the temperature structure of the fully equilibrated state. Green (1970) and Stone (1972) proposed such parameterizations for the case when β effects are small, while Held (1978) proposed such a parameterization for the case when β effects are large. Branscome (1983) combined Stone's and Held's parameterizations into a single parameterization valid for any β. Recently, an alternate parameterization, valid for any β, has been

proposed by Held and Larichev (1996). These parameterizations all differ in how the eddy flux depends on the temperature structure. In particular, the proposed dependences are as follows:

$$[\overline{v^*\theta^*}]^{pt} \propto \left(\frac{dT_e}{dy}\right)^2 \left(\frac{d\theta e}{dz}\right)^{-1/2} \quad \text{(Green 1970),} \quad (1a)$$

$$[\overline{v^*\theta^*}]^{pt} \propto \left(\frac{dT_e}{dy}\right)^2 \left(\frac{d\theta e}{dz}\right)^{+1/2} \quad \text{(Stone 1972),} \quad (1b)$$

$$[\overline{v^*\theta^*}]^{pt} \propto \left(\frac{dT_e}{dy}\right)^5 \left(\frac{d\theta e}{dz}\right)^{-5/2} \quad \text{(Held 1978),} \quad (1c)$$

and

$$[\overline{v^*\theta^*}]^{pt} \propto \left(\frac{dT_e}{dy}\right)^4 \left(\frac{d\theta e}{dz}\right)^{-3/2} \quad \begin{array}{l}\text{(Held and} \\ \text{Larichev 1996).}\end{array} \quad (1d)$$

A second class of parameterizations assumes that eddy effects can be taken into account implicitly by adjusting the temperature and/or the potential vorticity structure of the equilibrated state [Stone 1978; Lindzen et al. 1980; Gutowski 1985; Gutowski et al. 1989). Indeed, the possibility that the potential vorticity is homogenized by such an adjustment was a major motivation for this study. As we have seen, such a homogenization does occur in our model in the lower troposphere above the ABL. This adjustment implies an adjustment in the isentropic slope (Stone and Nemet 1996). In a quasigeostrophic system with specified static stability, this in turn implies a particular adjustment in the horizontal temperature gradient. However, as we have seen, when an interactive static stability is included, the horizontal temperature gradient and static stability adjust jointly so as to homogenize the potential vorticity near the 700-hPa level, but this does not require any particular adjustment in the gradient or the static stability. In this more general case, there remains the question of whether there may be an additional condition involving the horizontal and vertical temperature structure (besides no horizontal gradient of potential vorticity) to which the eddies adjust the temperature field.

First, we examine the dependence of the vertically averaged meridional eddy flux of potential temperature, $[\overline{v^*\theta^*}]^{pt}$, on temperature structure. Since the parameterizations given in Eq. (1) are based on scale statements, it is not obvious what values of the temperature gradient and static stability we should use when these quantities vary with height and latitude. In testing the parameterizations, we will somewhat arbitrarily use the measures of temperature structure given in Table 2, that is, the equilibrated structure at the center of the channel at the approximate level where the potential vorticity is homogenized. This is at least the location where the eddies interact most strongly with the mean flow.

A cursory examination of Table 2 shows that the parameterizations proposed by Held (1978) and Held and Larichev (1996) are too sensitive to the temperature structure to be consistent with our model results. For example, using the equilibrated temperature gradients given in Table 2, Held's parameterization [Eq. (1c)] predicts that $[\overline{v^*\theta^*}]^{pt}$ in experiment TZ1 should be 14.5 times larger than in experiment TZ4, while Held and Larichev's parameterization predicts that it should be 6.5 times larger. In fact, there is virtually no change in $[\overline{v^*\theta^*}]^{pt}$ between these two experiments.

On the other hand, parameterizations of Green (1970) and Stone (1972) are much less sensitive to the temperature structure. To test them, we plot in Fig. 8 for most of the experiments $\log([\overline{v^*\theta^*}]^{pt}/PD)$, where PD is one of the parameter dependences given in Eq. (1). If a parameterization were perfect, the plotted quantity would be a constant for all experiments. We see that Stone's (1972) parameterization comes closest to this ideal. For this parameterization, the mean value of $[\overline{v^*\theta^*}]^{pt}/PD$ for the experiments shown in Fig. 8 is 0.20, and the extreme differences from this value are on +21% and −25% even though the eddy heat flux varies by a factor of 14 over these experiments. For Green's parameterization, the mean of $[\overline{v^*\theta^*}]^{pt}/PD$ is 0.82, and the extreme differences from this value for the experiments shown in Fig. 8 are +42% and −41%. We also tested the parameter dependence PD $\propto (dT_e/dy)^2$, but this also did not do as well as Stone's parameterization.

We have excluded from the test shown in Fig. 8 the experiments TY8, RST, and LST. These experiments all involve changes in factors that may affect $[\overline{v^*\theta^*}]^{pt}$ aside from changes in the temperature structure in the region of homogenization. Experiment TY8 involves a change in the vertical structure of the forcing, which leads to stronger temperature gradients in the upper troposphere in TY8 than in SR, even though the gradients in the lower troposphere are identical (Fig. 2b). The only parameterization that explicitly attempts to allow for vertical variations in the temperature structure is Branscome's (1983). In particular, it uses a vertically weighted temperature gradient to calculate $[\overline{v^*\theta^*}]^{pt}$. Such a weighting would lead to a larger eddy heat flux in TY8 than in SR, qualitatively consistent with the results shown in Table 2. To get a more definitive check on the validity of such a weighting would, however, require more experiments than just TY8. In any case, the increased eddy heat fluxes in TY8 compared to SR can be attributed to the larger meridional temperature gradients in the upper troposphere.

Experiments RST and LST involve changes in the height of the tropopause, H. In Green's parameterization, $[\overline{v^*\theta^*}]^{pt}$ is independent of H, while in Stone's, it is proportional to H^2. However, the temperature structure at the levels of homogenization in these experiments also changes (Table 2), and furthermore, these changes are not characteristic of changes at other levels (Fig. 2e). Thus, to parameterize changes in $[\overline{v^*\theta^*}]^{pt}$ in
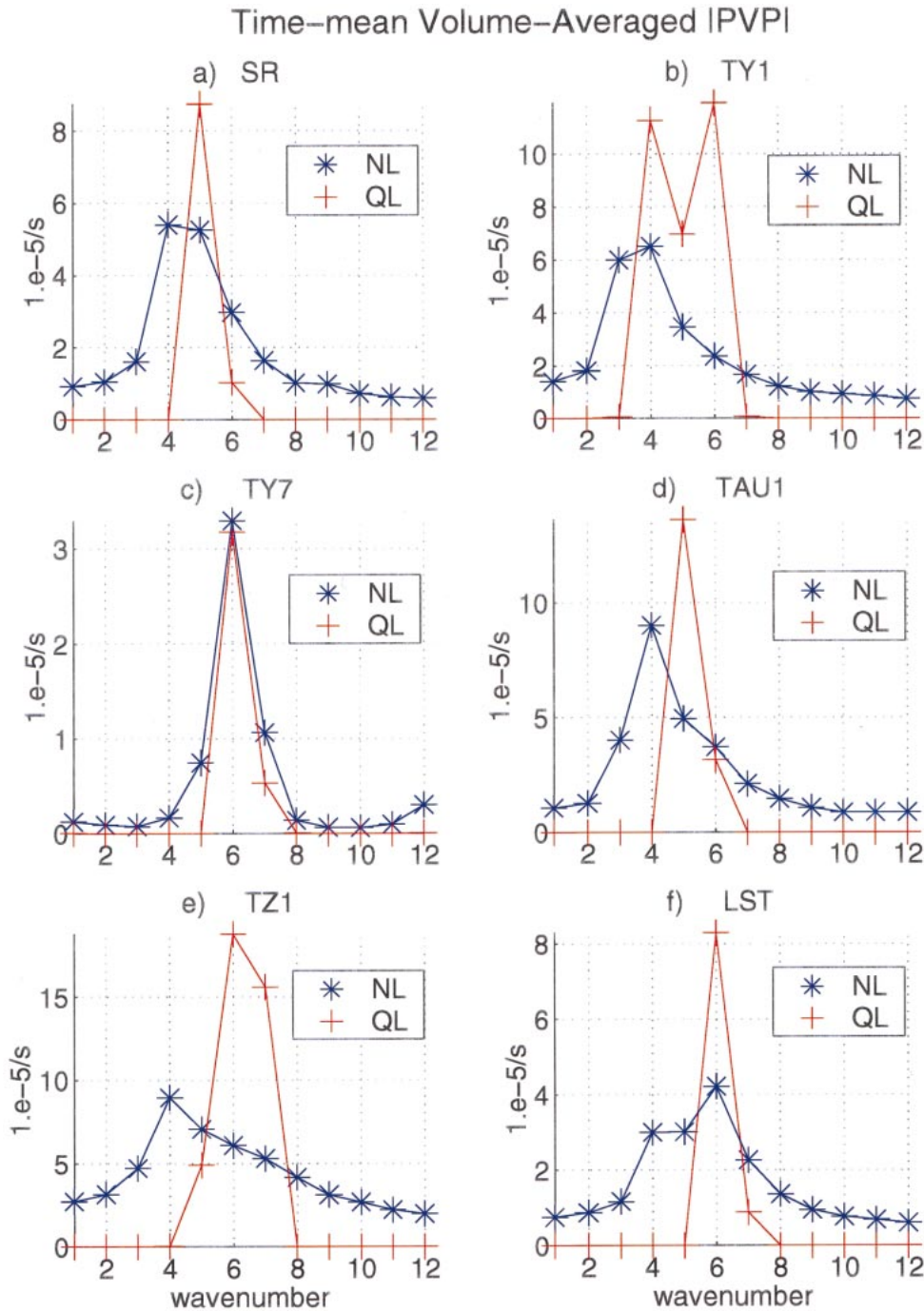
FIG. 6. Comparison between nonlinear and quasi-linear time–mean volume-averaged perturbation potential vorticity per wavenumber (in units of s^{-1}). The quasi-linear run has static stability fixed at the equilibrated nonlinear values.

these experiments would again require an appropriate vertical weighting as well as an appropriate dependence on H. These two experiments are not sufficient to get a good test of these multiple requirements. However, we note that the greater eddy heat flux in RST compared to LST does require that $[\upsilon^*\theta^*]^{pt}$ increase as H increas-es, since the meridional temperature gradient is smaller in RST, and the static stability is virtually the same. Thus the larger eddy heat flux in RST is qualitatively consistent with Stone's parameterizations but not Green's.

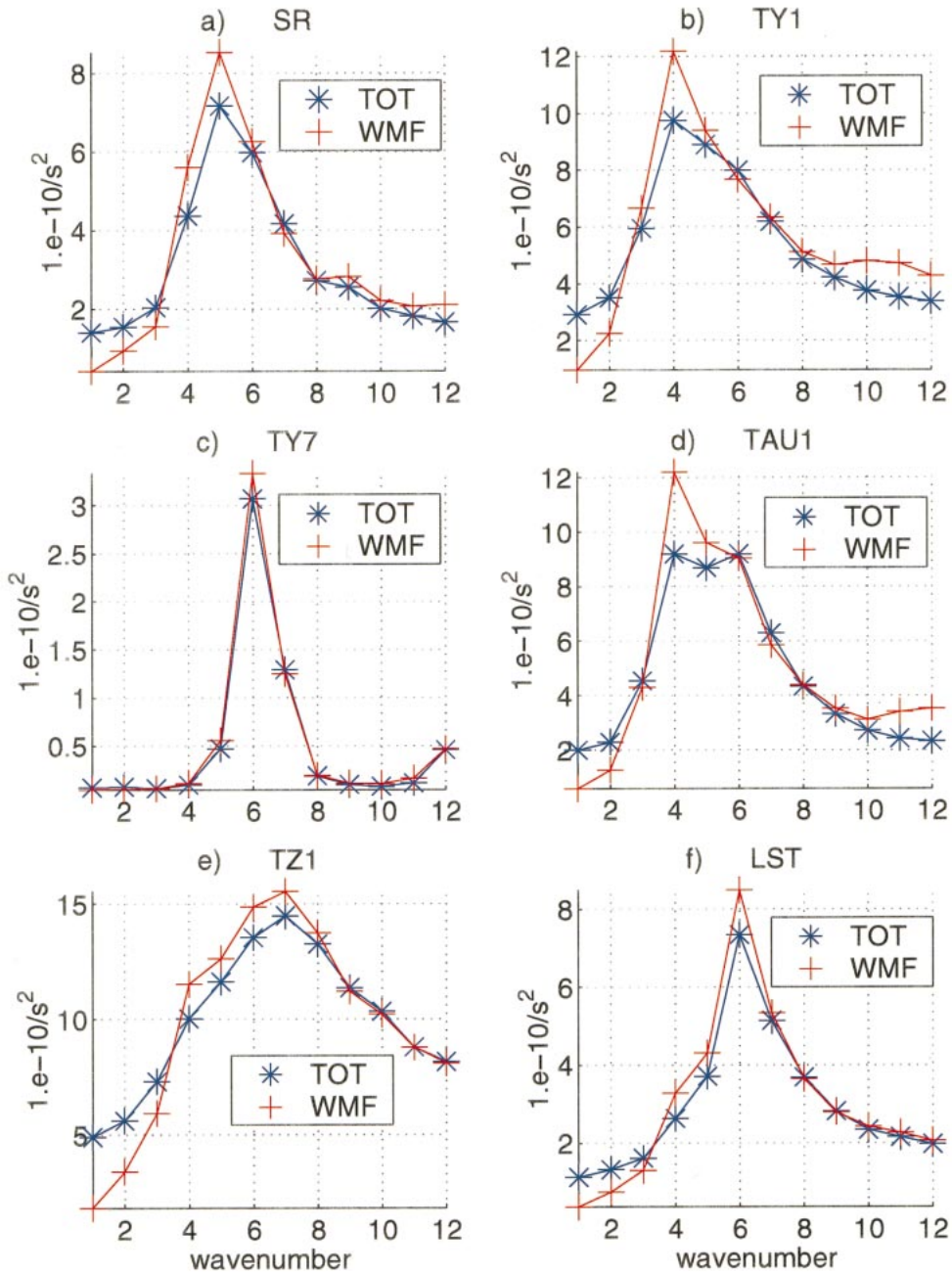We note that the fact that one of the parameterizations

FIG. 7. Comparison between total and wave–mean flow time–mean volume averaged PV fluxes
(in units of s^{-2}).

that neglects β effects works best in our model is likely to be an artifact of our having centered our β plane at 45°. Empirical tests show that the eddy flux is approximately proportional to the square of the meridional temperature gradient at 45°N (Stone and Miller 1980), consistent with Eqs. (1a) and (1b) and with our model results. However, at lower latitudes, it is more sensitive

to the gradient (Stone and Miller 1980). Thus, we would expect Held's (1978) and Branscome's (1983) parameterizations to be more appropriate at lower latitudes.

Finally, we consider the TAU experiments. None of the parameterizations of the eddy heat flux, Eq. (1), work for these experiments. By contrast, in these experiments, a very strong baroclinic adjustment appears
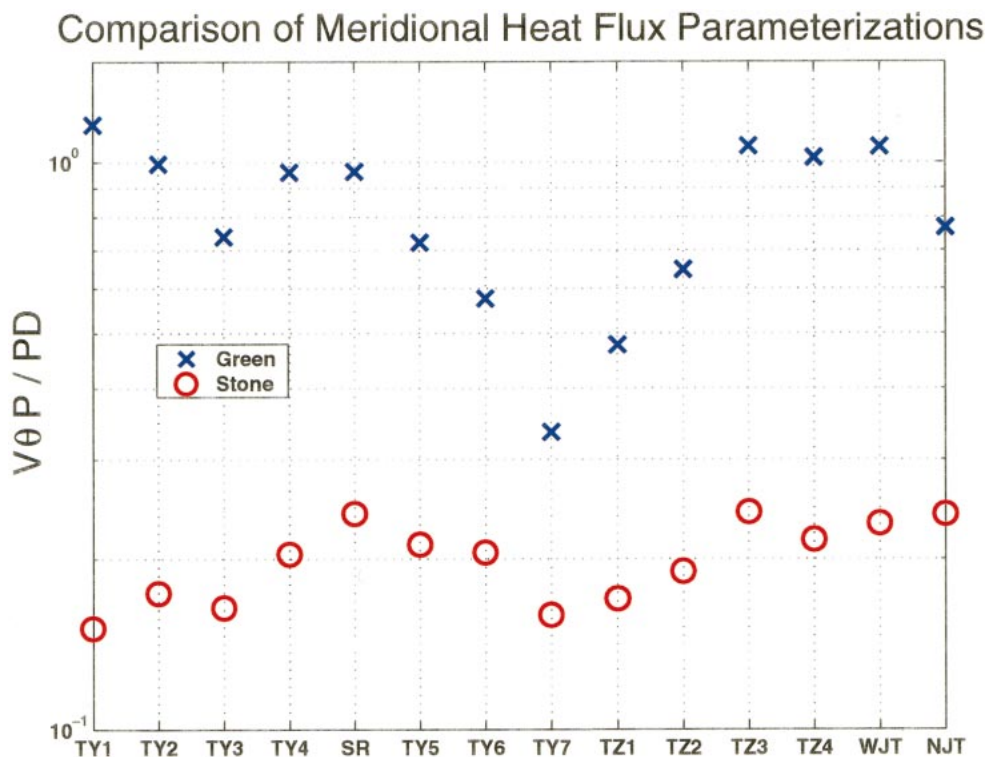
FIG. 8. The $\log([\overline{v^*\theta^*}]^{p,t}/PD)$ for Green's and Stone's parameterizations from the experiments indicated on the horizontal axis.

to be at work. Not only is the potential vorticity homogenized just above the ABL, but the meridional temperature gradient and static stability are also very robust throughout the troposphere, showing no appreciable change even though the relaxation time changes by a factor of 16 (Table 2). By contrast, there are large changes in the meridional and vertical eddy heat transports. These changes are just enough to offset the changes in diabatic heating and maintain the temperature structure. Why the TAU experiments should behave so differently from the other experiments is not apparent.

6. Discussion

This study has investigated the sensitivity of the equilibrated state of a multilevel quasigeostrophic β plane channel model to changes in forcing. We find that at the center of the channel, the potential vorticity just above the boundary layer is homogenized, and the PV gradients throughout the troposphere are insensitive to changes in forcing. We also found that the meridional temperature gradients and static stability were generally sensitive to changes in forcing. The changes to the meridional and vertical temperature structure work together in such a way that the PV gradients remain unchanged. The homogenization of the PV at the center of the channel above the ABL is quasi-linear in that it is accomplished by wave–mean flow fluxes. However, it is also

essentially nonlinear in that it does not occur unless the quasi-linearly unstable waves saturate and the nonlinear energy cascade shifts the wave–mean flow interaction to larger scales. If the forcing is sufficiently weak, then the homogenization does not occur, but for typical parameter values (as in our standard run), it does.

The equilibrated PV structure is significantly modified in the runs where the height of the tropopause is varied. These runs appear to be equilibrating to a different state than the other runs. The height of the tropopause is set by the forcing and the PV gradients increase approximately linearly with pressure from the minimum at the top of the ABL to the maximum at the tropopause. This quasi-linear increase with pressure is seen in all of the runs, and the dynamical reason for this is not clear. Lowering the height of the tropopause reduced the adjustment to the meridional temperature gradients and the static stability. This implies that knowing the temperature gradients at the top of the ABL is not enough to calculate the temperature structure of the free troposphere; it is also necessary to know the magnitude of the PV gradients at the tropopause and its height. This is not straightforward, since the eddy fluxes play a role in determining these two factors. Raising the tropopause actually increases the fluxes and the EKE.

The insensitivity of the PV gradients above the ABL to changes in forcing is useful because this equilibrated state may be used to characterize the net impact of the

eddies on the mean flow without necessarily determining what the fluxes due to these eddies are. If we assume that the height of the tropopause and the magnitude of the PV gradients at the tropopause are known, then the quasi-linear dependence of the PV gradients on pressure makes it possible to estimate the slope of the isentropes in the free troposphere. If the barotropic term in the PV gradients is small relative to the baroclinic term, then a simple expression for the isentropic slopes as a function of pressure throughout the free troposphere can be written in terms of the slope of the isentropes at the top of the ABL and the PV gradients at the tropopause.

Our results are qualitatively consistent with two-layer model results showing that nonlinearities shift the dominant eddy modes to larger scales, that this shift increases as the forcing increases and that the interaction of these dominant eddies with the mean flow is quasi linear. Even quantitatively, the sensitivities we find are similar to those in two-layer models, which include an interactive static stability (Zhou and Stone 1993b). However, two-layer models cannot resolve the homogenization of potential vorticity in the lower troposphere above the boundary layer present in our model.

Finally, we have used our model results to assess various parameterizations that have been proposed to represent the effects of eddies in an equilibrated flow. Stone's (1972) parameterization was the most successful at capturing changes in the meridional eddy heat flux over a wide range of experiments in which the forcing was varied. This success likely depends on the fact that our β plane model is centered at 45° latitude, and at this latitude, β effects are weak and the eddies are deep. Other parameterizations, which include β effects such as Held's (1978) and Branscome's (1983), are more likely to be successful at lower latitudes. However, even Stone's parameterization failed in the experiments in which the diabatic timescale was varied. In these experiments, both the homogenization of the potential vorticity in the lower troposphere above the ABL, and the temperature structure throughout the troposphere were remarkably robust.

REFERENCES

Bannon, P. R., and T. L. Salem Jr.,1995: Aspects of the baroclinic boundary layer. *J. Atmos. Sci.,* **52,** 574–596.

Branscome, L. E., 1983: A parameterization of transient eddy heat flux on a beta-plane. *J. Atmos. Sci.,* **40,** 2508–2521.

Cehelsky, P., and K. K. Tung, 1991: Nonlinear baroclinic adjustment. *J. Atmos. Sci.,* **48,** 1930–1947.

Gall, R., 1976: Structural changes of growing baroclinic waves. *J. Atmos. Sci.,* **33,** 374–390.

Green, J. S. A., 1970: Transfer properties of the large-scale eddies and the general circulation of the atmosphere. *Quart. J. Roy. Meteor., Soc.,* **96,** 157–185.

Gutowski, W. J., Jr., 1985: Baroclinic adjustment and midlatitude temperature profiles. *J. Atmos. Sci.,* **42,** 1733–1745.

——, L. E. Branscome, and D. A. Stewart, 1989: Mean flow adjustment during life cycles of baroclinic waves. *J. Atmos. Sci.,* **46,** 1724–1737.

Held, I. M., 1978: The vertical scale of an unstable baroclinic wave and its importance for eddy heat flux parameterizations. *J. Atmos. Sci.,* **35,** 572–576.

——, and V. Larichev, 1996: A scaling theory for horizontally homogeneous, baroclinically unstable flow on a beta plane. *J. Atmos. Sci.,* **53,** 946–952.

James, I. N., 1987: Suppression of baroclinic instability in horizontally sheared flows. *J. Atmos. Sci.,* **44,** 3710–3720.

Jin, F. F., and B. J. Hoskins, 1995: The direct response to tropical heating in a baroclinic atmosphere. *J. Atmos. Sci.,* **52,** 307–319.

Lindzen, R., B. Farrell, and K.-K. Tung, 1980: The concept of wave over-reflection and its application to baroclinic instability. *J. Atmos. Sci.,* **37,** 44–63.

Manabe, S., and F. Möller, 1961: On the radiative equilibrium and heat balance of the atmosphere. *Mon. Wea. Rev.,* **89,** 503–532.

Solomon, A., and P. H. Stone, 2001: Equilibration in an eddy resolving model with simplified physics. *J. Atmos. Sci.,* **58,** 561–574.

Stone, P. H., 1972: A simplified radiative-dynamical model for the static stability of rotating atmospheres. *J. Atmos. Sci.,* **29,** 405–418.

——, 1978: Baroclinic adjustment. *J. Atmos. Sci.,* **35,** 561–571.

——, and D. A. Miller, 1980: Empirical relations between seasonal changes in meridional temperature gradients and meridional fluxes of heat. *J. Atmos. Sci.,* **37,** 1708–1721.

——, and L. Branscome, 1992: Diabatically forced, nearly inviscid eddy regimes. *J. Atmos. Sci.,* **49,** 355–367.

——, and B. Nemet, 1996: Baroclinic adjustment: A comparison between theory, observations, and models. *J. Atmos. Sci.,* **53,** 1663–1674.

Welch, T. W., and K. K. Tung, 1998: Nonlinear baroclinic adjustment and wavenumber selection in a simple case. *J. Atmos. Sci.,* **55,** 1285–1302.

Zhou, S., and P. H. Stone, 1993a: The role of large-scale eddies in the climate equilibrium. Part I: Fixed static stability. *J. Climate,* **6,** 985–1001.

——, and ——, 1993b: The role of large-scale eddies in the climate equilibrium. Part II: Variable static stability. *J. Climate,* **6,** 1871–1880.